2025 IEEE World Haptics Conference (WHC)
Suwon Convention Center, Suwon, Korea
July 8 ~ 11, 2025

Reducing the Number of Actuators in Braille Displays with Time Reversal Focusing

Madoux Esteban
Université Paris Saclay
CEA, List
Palaiseau, France
https://orcid.org/0009-0004-9415-3485

Hudin Charles
Université Paris Saclay
CEA, List
Palaiseau, France
https://orcid.org/0000-0002-8065-5626

***Abstract*—Refreshable braille displays give visually impaired people access to text and graphics. Existing technologies typically use an actuator for each braille dot, making full-page displays complex, cumbersome and costly, and ultimately limiting their use. This paper presents a novel methodology for actuating a large number of braille pins with a small number of actuators. Each braille pin comprises a bistable mechanism that is actuated through time reversal focusing of elastic waves. The design of such a system is studied in detail, and a mock-up device has been constructed in order to implement the method. The system is able to operate several braille pins one at a time from remote actuators. Although the repeatability of the process still requires improvements, the measurements show a good agreement with theory and allow us to envisage a full-page display based on this method.**

***Index Terms*—refreshable braille display, time reversal wave focusing, wave propagation, bistable mechanism.**

I. Introduction

Digital content is mostly visual and thus inaccessible to blind and low vision people. Text-to-speech synthesis and screen reader technologies have made significant progress and offer relevant solutions for accessing textual content and for navigating graphical user interfaces through audio. The audio modality however does not lend itself easily to the rendering of 2D content such as graphics, maps and images. In addition to text to speech, accessing text by actively reading braille remains fundamental and plays a role in the development of literacy. The sense of touch thus remains a key sensory substitution modality and the development of devices able to display braille and graphical contents in the form of raised dots patterns can still play a role for accessibility.

The braille alphabet encodes letters, numbers and musical notes in the form of raised dots on a 2×3 or 2×4 grid, depending on the purpose. Although different standards exist [1], [2], the typical distance between dots on refreshable braille displays is 2.3 to 2.5 mm, for a dot base diameter of 1.5 to 1.6 mm and a raised dot height of 0.6 to 0.9 mm. For refreshable displays, the dot holding force is also a key feature to withstand the finger pressing force. The American Center for Braille Innovation [3] recommends a minimum of 0.25 N lifting force. This value is also shared by [4], which gives a target blocking force between 0.2 and 0.5 N. Despite the simplicity of the mechanical function: raising or lowering a dot, the combined requirement of pin count, density, stroke and holding force make the subject challenging and the design of refreshable braille displays remains an active topic of research. Different technologies are either commercialized or under research with different display size using different principles: magnetism [5], fluids [6], [7], pneumatic [8], piezoelectric [9], [10], shape-memory alloy [11], [12], etc. These technologies share the issue of using one actuator per braille dot. This somehow simplifies the design and maintenance while offering a high refresh rate and responsiveness. However, this leads to complex, cumbersome and costly device with reported price around 100 $ per braille cell for commercially available displays [13]. Some devices and research focus on reducing the price by reducing the number of actuators. This can be achieved by pooling them, that is operating several Braille dots from a single actuator. This idea can be seen in commercial product like the Canute 360 [14] or in research with the work of [15] on sliding actuators. In these works, the introduction of a latching mechanism dissociates the function of changing the pin state, which requires energy over a short period, and the passive and long-standing function of holding the pin in place. This enables to mutualize the actuators but requires a new mechanism to move this actuator.

To avoid this difficulty, we explore in this work the possibility to use mechanical waves as a mean of delivering energy to the pins, designed to exhibit a bistable behaviour. With this approach, a few actuators can be placed remotely and mutualized to control pin states. The number and density of actuator can thus be dramatically reduced while preserving a high refresh rate. This work presents the principle, derives design trade-off and demonstrates the ability to change the state of any chosen pin remotely. The demonstration is made on a mock-up device with 96 braille pins and 32 actuators. The mock-up has a pin-to-pin distance of 2.5 mm, a holding force of 0.3 N, a pin extrusion of 0.5 mm and a refresh rate of 500 pin switch per second. It paves the way to the design of a full-page refreshable display of thousands of pins controlled by only 32 actuators.

We gratefully acknowledge support from the EU for the Horizon project ABILITY, grant no 101070396.

II. PRINCIPLE

A. Time reversal wave focusing

Time reversal is a signal processing method that enables the focusing of waves at any chosen position from a set of distant actuators. By taking advantage of the time symmetry of wave equations, this method makes the focusing of energy particularly easy even in complex propagation medium. It was first introduced by [16] for medical ultrasound application but has since found application in all fields of wave physics. Several implementations in haptics have already been proposed to localized stimuli on interactive surfaces [17], [18], [19]. During the time reversal operation, out of plane vibrations generated by the different actuators propagate within the plate, interfere with scatterers and reflect on the plate boundaries. After a few milliseconds typically, all the waves converge at the focus point; the vibrations interfere constructively to generate a localized velocity peak that last typically a few microseconds and finally diverge and attenuate in the plate.

To display braille, we harness the kinetic energy concentrated at focus point and time to toggle the state of a pin between a low and a high position.

B. Bistable pins

A refreshable braille display must provide a surface where pins are either in an upper state or a lower state. In the upper state, the pin should protrude from a reading surface (i.e. a plate that is touchable by the user) and withstand the finger-pressing force. In its lower state, the braille pin must disappear below the surface.

Bistable structures are present in biological systems, such as in the natural fly trap [20] and in technological systems to store energy [21] or information [22]. There are many ways of obtaining bistable mechanisms but their potential energy profile shows common features. A bistable structure is a system that exhibits two stable states, each corresponding to a local minimum of potential energy. To transition between these states, the system must overcome an energy barrier through an external energy input. Therefore, toggling from one stable state to the other requires an energy input larger than the energy barrier ΔE. Among the many options for designing a bistable system, we chose to combine two permanent magnets connected by a rod through a ferromagnetic plate, as depicted in Fig. 1. With this design, the pin assembly stabilizes in high or low position and always maintains a contact with the ferromagnetic plate, while the use of neodymium magnets generates sufficient force within a small volume.

C. The refreshable display

The central ferromagnetic plate serves as a waveguide in which mechanical waves propagate. With time reversal focusing, an impulsive surface motion can be produced upward or downward by simply reversing the sign of the driving signals. When the pin is in low state, a pulse directed upward pushes the pin up. When the pin is in high state, a pulse directed downward pushes the pin down.

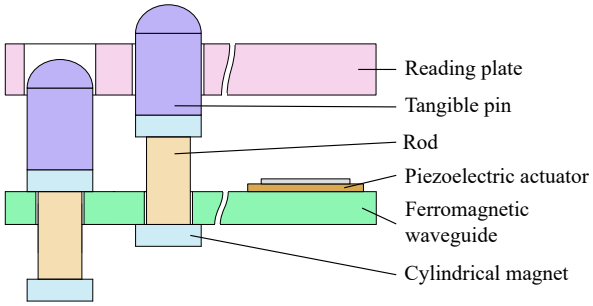

Fig. 1. System architecture: Each tangible pin is mounted on a bistable assembly composed of two permanent magnets connected by a rod through a ferromagnetic waveguide. Remote piezoelectric actuators generate and focus waves at the dot position.

The order of magnitude of the plate displacement at focus point is in the µm order but the velocity can reach values in the m/s range, due to the possibly high frequency bandwidth. A pin at focus point therefore acquires a significant amount of kinetic energy at focus time. If this kinetic energy $E_c = \frac{1}{2}Mv^2$ is sufficient and the velocity impulse directed correctly, the pin overcomes the energy barrier ΔE and toggles to its other stable state, in high or low position. The critical speed that must be reached at focus point to toggle the pin is thus:

$$v = \sqrt{\frac{2\Delta E}{M}} \tag{1}$$

With ΔE the energy barrier and M the pin mass. The overall system architecture is detailed in Fig. 1. In addition to the bistable pin and ferromagnetic plate, piezoelectric actuators are placed at the plate periphery to generate and control bending waves. Tangible pins are placed on top of the bistable assembly and protrude through a reading plate to contact with user fingers.

III. DESIGN TRADE-OFFS

A. Bistable pin design

To fulfil the requirement of the braille refreshable display presented in section I, the bistable mechanism must resist a 0.25 N force applied to it. According to the manufacturer's datasheet [23], a 1.5 mm diameter, 0.5 mm thick cylindrical neodymium magnet with an axial magnetization of N45 exhibits an adherence force of approximately 0.32 N, which satisfies the bistable mechanism's requirements. Therefore, the bistable mechanism comprises two of these magnets separated by a rod and associated with a ferromagnetic plate. The total pin run and plate thickness determine the length of the rod. From the requirements presented in the introduction, we want the pin to protrude from the reading plate by at least 0.6 mm. However, we want to avoid any accidental switch down caused by a user force higher than the magnetic holding force. Therefore, we chose to double the pin run to 1.25 mm and let it protrudes by 0.6 mm. This way, pins cannot be pushed manually low enough to toggle to its low state.

B. Waveguide design

Once the geometry and the design of the bistable system are achieved, we can look at the design of the waveguide. To toggle a pin without affecting the state of its neighbours, the velocity must exceed the critical speed only at the focus point. We therefore target a focusing resolution R_s, or half-amplitude spot size, equal to the pin-to-pin distance. With this resolution, pins adjacent to the controlled one reach at most half of the peak velocity, thus providing a safety margin to accommodate the variability of pin assembly. We, therefore, aim at $R_s = \frac{\lambda_{min}}{2} = p$, with λ_{min} the smallest wavelength controlled by the focusing operation and $p = 2.5\,\text{mm}$ the pin-to-pin distance.

To focus at the desired position, bending waves must propagate from actuators at the periphery of the plate to the heavier area covered with pins. On their way, waves therefore encounter an impedance jump, which results in a transmission loss and reduced wave amplitude. We seek to minimize this impedance difference to maximize the transmission of waves. The transmission coefficient for waves travelling from a medium of impedance Z_1 to another of impedance Z_2 is [24]:

$$T = \frac{2Z_1}{Z_1 + Z_2} \tag{2}$$

Which in the case of thin plates simplifies, see [25], in:

$$T = \frac{2k_1^2}{k_1^2 + k_2^2} \tag{3}$$

with k_1 and k_2 the wavenumbers in the propagation medium at the selected frequency. For homogeneous thin plates, the dispersion equation writes [26]:

$$k_i^2 = \sqrt{\frac{\rho_i}{D_i}\omega} \tag{4}$$

With ω the circular frequency and ρ_i and D_i the surface density and rigidity respectively. At low frequency, the pin covered area can be seen as homogeneous with a mass density:

$$\rho_2 = \rho_1 + \frac{M}{p^2} \tag{5}$$

With M the pin mass, ρ_1 the surface density of the plate, ρ_2 the equivalent density in the pin covered area and p the pin distance. However, as the frequency increases, we must consider the discrete nature of pins that form a periodic array of scatterers for the flexural waves. Such periodic medium constitutes a phononic crystal with unique properties such as frequency bandgaps at which waves cannot propagate inside the medium. Bragg bandgaps appear for wavelengths equal to twice the array period while resonant bandgaps appear at the resonant frequency of the scattering elements [27]. Those resonant bandgaps find applications in haptics to provide vibration isolation or to design waveguides [28]. In our case, however, they would hinder the transmission of waves.

The design procedure consists in optimizing the transmission coefficient with the homogeneous model while avoiding resonance of the pin within the frequency range of interest. To that end, we increased the stiffness of the pin rods by selecting a metallic material. Brass has the advantage of having a high density, which in virtue of equation (1) decreases the required velocity. It is also non-ferromagnetic and does not interfere with the magnetic field. We fixed the rod diameter to 1 mm. In a first approximation, we assume that the tangible part of the pin will be in plastic and we neglect its weight. The pin mass thus writes:

$$M = 2m + \rho_r d_r^2 \frac{\pi}{4} e_r \tag{6}$$

The pin mass is indeed the addition of magnet masses m and rod mass with density ρ_r, diameter d_r and height e_r. The plate thickness e_p and rod height e_r are related to the target pin run r by the relation $r = e_r - e_p$. We finally obtain:

$$M = 2m + \rho_r d_r^2 \frac{\pi}{4} (r + e_p) \tag{7}$$

Combining equations (3), (4), (5), and (7) gives the expression of a transmission coefficient as a function of plate thickness shown in Fig. 2. We finally selected a plate of thickness 0.75 mm to attain a transmission ratio of 90 % between the periphery and the central part of the plate. To validate further this choice, we can use semi-analytical results for an array of point resonators on a thin plate. From [29], we calculate the dispersion relation in a thin plate with periodically attached spring-mass resonators. From the obtained wavenumbers we calculate with (3) the transmission ratio as a function of frequency in the case of a plane wave impinging the pin array with normal incidence. The wavelength $\lambda_{min} = 2p$ is reached for a dimensionless wavenumber (or reduced wavenumber) $\frac{kp}{\pi} = \frac{2\pi}{\lambda_{min}}\frac{p}{\pi} = 1$, which in our case corresponds to a frequency of 210 kHz. We notice in Fig. 3 that the homogeneous model gives a reasonably good approximation of the transmission ratio even for wavelengths as short as twice the pin distance. To illustrate the importance of avoiding pin resonance, we calculate the transmission ratio for the same plate but with pin exhibiting a resonant frequency at 50 kHz. We observe on Fig. 3 that the target wavelength, for which $\frac{kp}{\pi} = 1$, is reached within the pin array at a lower frequency. The transmission coefficient is strongly reduced over the whole bandwidth, thus making ineffective the actuation from remote source.

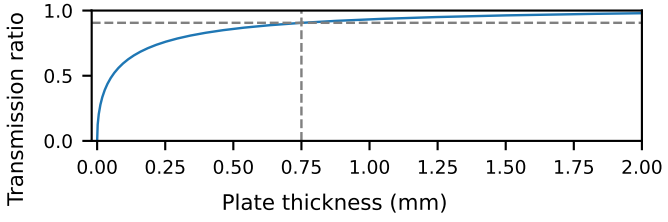

Fig. 2. Wave transmission ratio at the interface between free and pin covered areas of the plate. For the chosen pin, a plate thickness of 0.75 mm gives a satisfactory transmission of 90 %.

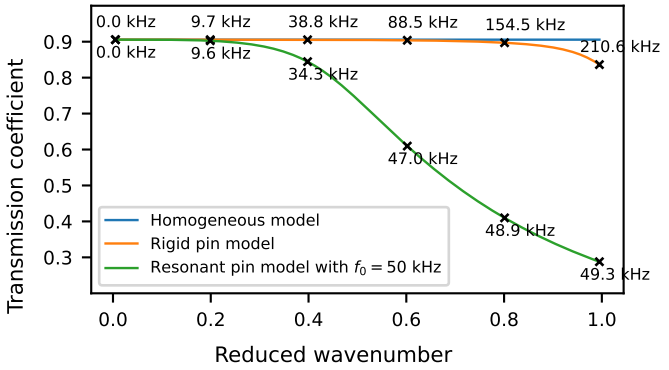

Fig. 3. Transmission coefficient with the homogeneous model (blue), the discrete model with rigid pin (orange), and discrete model with resonant pin (green) as a function of reduced wavenumber and frequency. The pin resonance induces a reduction in the transmission ratio.

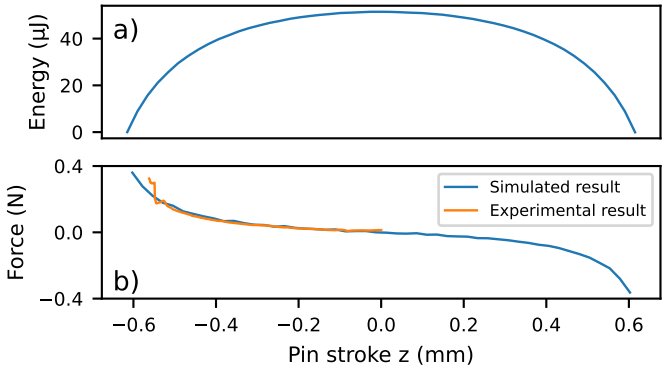

Fig. 4. a) Evolution of the simulated magnetic energy of the system with a potential energy barrier of 51 µJ. b) Evolution of the simulated and experimental data of the force on the system. The maximum simulated value is 0.37 N and the experimental value reached 0.32 N.

IV. Prototype Description

A. Bistable pins

Verifying the system's performance is important once the different parts are designed and sized. One crucial parameter is the holding force of the pin. To ensure that the pin would switch, we did a simulation using Agros2D [30], a finite element method simulation software. We used an axisymmetric simulation to obtain the magnetic energy profile of a single pin as it moves from one state to the other. Fig. 5 shows the geometry of the pin. From the energy profile, we derive the magnetic force with the expression $F = \frac{dE}{dx}$ with z the vertical axis of the pin.

We compared those theoretical force values with the actual force on a dedicated bench. We used a voice coil cylinder (Physik Instrument V-275.431) to push the pin downward. The voice coil is controlled in position and speed and simultaneously measures the force. Fig. 4 shows the evolution of the simulated energy of the system and the simulated and experimental data of the force on the system. Only the first half of the force profile was experimentally acquired as the second half corresponds to negative pulling force that would require gluing the tip of the voice coil cylinder to the pin. On the simulation, the maximum force is 0.37 N. This value is higher than the one given by the manufacturer of 0.32 N [23]. The presence of a coating on magnets might be the cause of this discrepancy as it adds a gap between the ferromagnetic plate and the magnet and reduces the magnetic force. The experimental force value is also lower than the simulated one but agrees very well with the manufacturer's data, with a maximal value at the beginning of the push at 0.32 N. This confirms that the presence of a hole under the magnet does not affect significantly the holding force. Finally, the simulated and measured forces show a remarkable agreement and the proposed design complies with the required pin force and run. The simulation indicates an energy barrier of $\Delta E = 51\,\mu\text{J}$ for this pin assembly. With a pin mass of $M = 26\,\text{mg}$ we obtain a critical speed $v_c = 2\,\text{m/s}$.

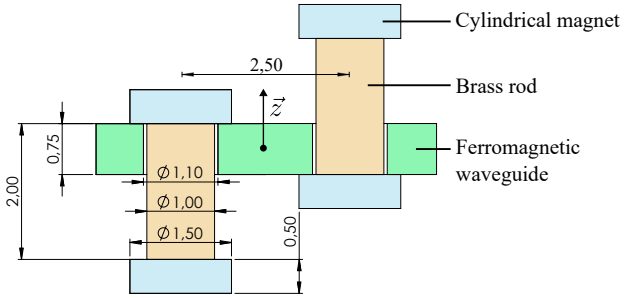

Fig. 5. Schematic of the bistable mechanism: composed of two cylindrical magnets linked by a brass rod through a ferromagnetic waveguide.

B. Prototype

The waveguide plate is made of a ferromagnetic steel plate of $200 \times 300 \times 0.75\,\text{mm}$ bonded to a rigid wooden frame by a 6 mm wide adhesive foam. The plate Young's modulus is $Y = 210\,\text{GPa}$, the Poisson's ratio is $\nu = 0.3$, the density is $\rho = 7800\,\text{kg/m}^3$. This first prototype is dedicated to proof of concept with ninety-six Braille pins arranged in 3 rows and 32 columns, forming 16 Braille characters. These 96 Braille pins are placed in the upper left corner of the plate. The full prototype intends to have 4800 Braille pins arranged in 60 rows and 80 columns on the same plate's dimensions actuated by the same 32 actuators. We placed these 32 actuators at the edge of the plate glued with an epoxy glue referenced 3M DP-490. The actuators are piezoelectric buzzer-type actuators referenced 7BB-20-6-L0 from Murata. These actuators are placed to avoid symmetries that could reduce the focusing quality. Fig. 6 presents a schematic of the prototype. This prototype is missing the tangible pin and the reading plate mentioned in Fig. 1 as only the actuation is tested here. The weight added by the tangible pin is low compared to the bistable mechanism. The driving electronics is a single-bit switching electronics identical to the one used by [17]. The values of the output RLC filter are, however, different. The capacitance of the actuator is $C = 10\,\text{nF}$, the resistor's value is $R = 10\,\Omega$, and the inductor's value is $L = 10\,\mu\text{H}$.

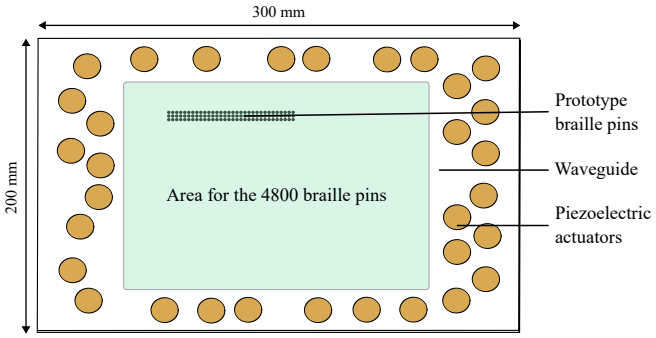

Fig. 6. Schematic of the mock-up device with 32 piezoelectric actuators, a ferromagnetic waveguide and 96 braille pins arranged in a 3×32 matrix.

V. Prototype Evaluation

A. Calibration procedure

Time reversal requires a prior calibration of the system, as described in [17]. Each piezoelectric actuator at a time is driven with a linear swept sine of duration 100 ms with a frequency up to 400 kHz sampled at 800 kHz. A sigma delta modulation at 4 MHz is then applied to reduce the single-bit quantization noise. Synchronously to the emission, a laser vibrometer (Polytec OFV-2500) records the out of plane velocity $v(t)$ of the pin of interest. This process is repeated for each actuator q and each pin i of the prototype.

B. Calibration results

From data acquired in the calibration step we can first observe the frequency response. With the swept sine on actuator q defined as $u_q(t)$ and the velocity of pin i as $v_i(t)$, the impulse response $H_{iq}(\omega)$ is defined as:

$$H_{iq}(\omega) = \frac{\text{FFT}\left(v_i(t)\right)}{\text{FFT}\left(u_q(t)\right)} \tag{8}$$

Fig. 7 shows the evolution of the amplitude of the signal for one actuator in blue, and the Root Mean Square (RMS) of all the points and all the actuators in orange. In this figure, we can see an attenuation of the signal after 200 kHz caused by the RLC output filter of the electronics. The small drop between 50 kHz and 80 kHz is likely due to a non-radiating effect [31]. The next interesting data to plot is the impulse response of the plate in the temporal domain. By doing the inverse Fourier operation of $H_{iq}(\omega)$, we can obtain $h_{iq}(t)$, which represents the transfer function in the time domain of the plate. Fig. 8 shows the impulse response of one signal in blue and the RMS signal of all signals (i.e. all actuators and all points on the plate) in orange. The fitted exponential attenuation curve with a time constant of attenuation τ=0.8 ms is shown in gray. To obtain the maximum focusing amplitude, the time reversal window duration is typically set to $T = 3\tau$. The system refresh rate is therefore directly related to this attenuation constant. We chose a time reversal duration of T=2 ms, nearly 3 times the attenuation time, as a trade-off between focusing amplitude and refresh rate. To focus at a

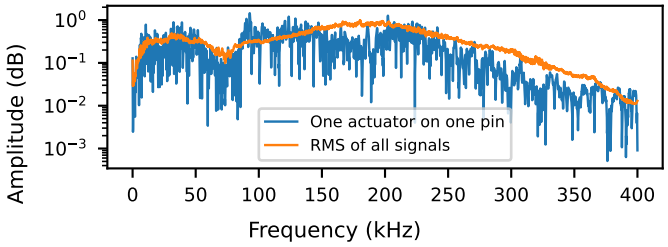

Fig. 7. Evolution of the amplitude of the signal for one actuator in blue and the Root Mean Square (RMS) of all points of all actuators in orange in the Fourier domain. An attenuation after 200 kHz comes from the electronics, and the drop between 50 kHz and 80 kHz is probably due to a non-radiating ultrasonic vibration.

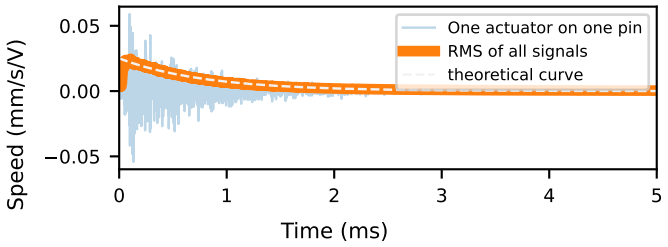

Fig. 8. Evolution of the speed of the signal for one actuator in blue and the RMS of all points of all actuators in orange in the temporal domain. In grey is plotted the theoretical curve of the dispersion of the waves in the plate with a time constant equals to 0.8 ms.

position i, each actuator is driven with a signal $s_q(t)$ that correspond to the time-reversed impulse response h_{iq}. We finally quantize this signal over a single bit to comply with our electronics and increase the focusing amplitude [17].

$$s_q(t) = V_p \text{sign}\left(h_{iq}(T-t)\right) \tag{9}$$

The theoretical response to this driving voltage on any pin can be obtained by computing the convolution with this signal as:

$$u_j(t) = \sum_{q=1}^{32} \left(h_{jq} \circledast s_q\right)(t) \tag{10}$$

The result of this equation is plotted at the focus point (i.e. for $i = j$) in Fig. 9. It represents the theoretical velocity of the focused pin for a peak voltage $V_p = 1$ V. We clearly observe the focusing at time $t = 2$ ms with a peak value of 150 mm/s.

The response at the focus time ($t = T$) for all other pin (i.e. for $i \neq j$) can be calculated to observe the spatial resolution plotted in Fig. 10. By low-pass filtering the driving signals at frequencies 20 kHz, 70 kHz, 150 kHz and 200 kHz we observe the effect of the signal frequency on focusing resolution and ensure that adjacent pins can be actuated independently. Fig. 10 and Fig. 11 show that increasing the band-pass frequency affects both the peak velocity and the resolution. With an upper frequency above 150 kHz, the peak velocity of adjacent pins is less than half the peak amplitude at focused position. This value is lower than the predicted value from section III-B (210 kHz) but validates the order of magnitude and the ability to control adjacent pins individually.

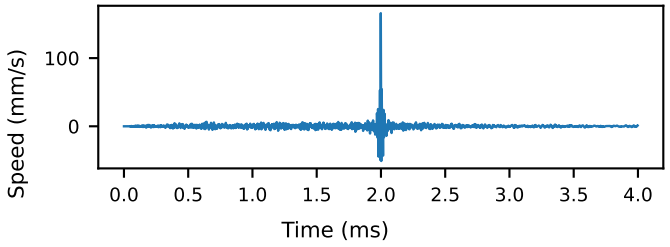

Fig. 9. Simulated speed of the time reversal wave focusing at the focus point as a function of time. The focalisation appears at time $t = 2\,\text{ms}$ with a peak value of 150 mm/s for a peak voltage $V_p = 1\,\text{V}$.

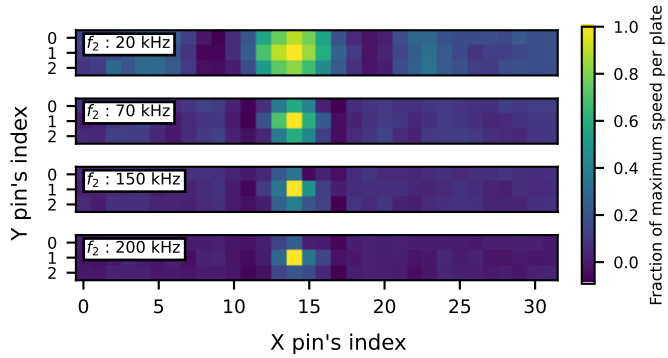

Fig. 10. Theoretical response of the plate to focusing on a pin for different high frequencies of the band-pass filter at focusing time (t=T): increasing the frequency decreases the spatial resolution of the time reversal.

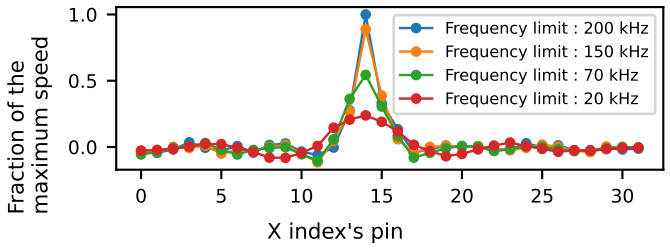

Fig. 11. Theoretical cross-section of the response of the plate to focusing on a pin for different high frequencies of the band-pass filter at focusing time.

C. Pin actuation

Finally, we focused over different pins with a peak voltage of 60 V and measured the resulting pin position and velocity. Two typical results are shown Fig. 12 that show the pin motion when the initial pin velocity is above or bellow critical speed. In both cases the velocity profile differs from the theoretical curve of Fig. 9 that assumes a pin rigidly fixed to the plate. In the experimental measurement, we observe at $T = 1.56\,\text{ms}$ a very fast increase of the pin velocity caused by the focusing reaching 2.3 m/s. When this value is higher than the critical speed $v_c = 2\,\text{m/s}$ calculated in section III-A, the pin swaps to its higher position. In the first phase of the motion ($T = 1.56\,\text{ms}$ to $1.8\,\text{ms}$) the pin is slowed down by magnetic force that retain it to the low state. From $1.8\,\text{ms}$ the upward magnetic force on the low magnet dominates the downward force on the high magnet. After this time the pin is attracted to its high position and accelerates until it hits the plate around $T = 2.3\,\text{ms}$, thus completing the state change. The negative velocity peak at the end is the deceleration of the pin once it touches the plate. This behaviour is confirmed in Fig. 12 b) that shows an increasing pin position that stabilizes at 1.2 mm. We faced difficulties in the realisation of the device leading to assembly imperfections and misalignment of pin components, owing to their small size that brought a significant variability in the behaviour of the assembled pins. For this reason, we were not able to actuate all of the 96 pins in both directions as expected each time. Most of them were able to switch in both directions with little repeatability. Yet, a companion video shows the successive motion of several pins on the central row and demonstrates the validity of the approach. The driving signal were set to put those pins in the upper position one after the other. Unfortunately, only a fraction of them responded as expected to the focusing, owing to assembling difficulties. In particular, the video shows a magnet moving laterally in response to plate vibrations, having become desolidarized from its rod. This illustrates the difficulty to assemble reliably such small components.

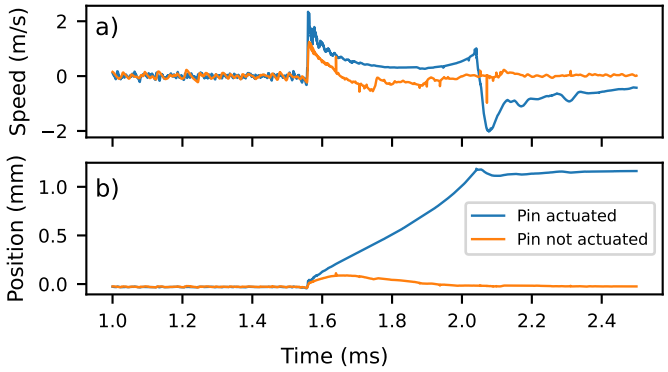

Fig. 12. Evolution of the pin veolcity a) and position b) as a function of time during the time reversal wave focusing. The blue curve is for a pin successfully actuated and the orange curve is for a pin where the kinetic energy transmitted from the plate to the pin was not sufficient.

VI. Conclusion

We introduced in this paper a method to control remotely the high or low state of bistable pins from focused ultrasonic vibrations. The theoretical analysis of the method enabled to draw design guidelines and attain the dimensional and strength requirements for displaying Braille. The measurements carried on a mock-up device demonstrate the feasibility of the approach although only a fraction of dots could be successfully moved. These initial results let us believe that a full-page refreshable braille based on this principle is achievable with the potential to make this type of device more accessible and compact. Beyond braille displays, the ability to reconfigure a multistable structure from a reduced set of remote actuators seems appealing for reconfigurable surfaces and robotics applications.

REFERENCES

[1] J. Brown, "Specification 800:2014 Braille Book and Pamphlets," Oct. 2014.

[2] "ISO 17049 Accessible design — Application of braille on signage, equipment and appliances," Oct. 2013.

[3] "EAP Braille Display Needs and Requirements," https://studylib.net/doc/18655312/eap-braille-display-needsand-requirements.

[4] D. Leonardis, L. Claudio, and A. Frisoli, "A Survey on Innovative Refreshable Braille Display Technologies," in *Advances in Design for Inclusion*, G. Di Bucchianico and P. F. Kercher, Eds. Cham: Springer International Publishing, 2018, pp. 488–498.

[5] J. Kim, B.-K. Han, D. Pyo, S. Ryu, H. Kim, and D.-S. Kwon, "Braille Display for Portable Device Using Flip-Latch Structured Electromagnetic Actuator," *IEEE Transactions on Haptics*, vol. 13, no. 1, pp. 59–65, Jan. 2020.

[6] Jun Su Lee and S. Lucyszyn, "A micromachined refreshable braille cell," *Journal of Microelectromechanical Systems*, vol. 14, no. 4, pp. 673–682, Aug. 2005.

[7] P. Goethals, H. Lintermans, M. M. Sette, D. Reynaerts, and H. Van Brussel, "Powerful Compact Tactile Display with Microhydraulic Actuators," in *Haptics: Perception, Devices and Scenarios*, D. Hutchison, T. Kanade, J. Kittler, J. M. Kleinberg, F. Mattern, J. C. Mitchell, M. Naor, O. Nierstrasz, C. Pandu Rangan, B. Steffen, M. Sudan, D. Terzopoulos, D. Tygar, M. Y. Vardi, G. Weikum, and M. Ferre, Eds. Berlin, Heidelberg: Springer Berlin Heidelberg, 2008, vol. 5024, pp. 447–457.

[8] X. Wu, S.-H. Kim, H. Zhu, C.-H. Ji, and M. G. Allen, "A Refreshable Braille Cell Based on Pneumatic Microbubble Actuators," *Journal of Microelectromechanical Systems*, vol. 21, no. 4, pp. 908–916, Aug. 2012.

[9] F. J. Tieman and K. Zeehuisen, "TACTILE RELIEF DISPLAY DEVICE AND METHOD FOR MANUFACTURE IT," Netherlands Patent 4,758,165, 1988.

[10] T. Völkel and G. Weber, "Tactile Graphics Revised: The Novel BrailleDis 9000 Pin-Matrix Device with Multitouch Input," in *Computers Helping People with Special Needs: 11th International Conference, ICCHP 2008*, vol. 11. Linz, Austria: Springer Berlin Heidelberg, Jul. 2008, pp. 835–842.

[11] N. Besse, S. Rosset, J. J. Zárate, E. Ferrari, L. Brayda, and H. Shea, "Understanding Graphics on a Scalable Latching Assistive Haptic Display Using a Shape Memory Polymer Membrane," *IEEE Transactions on Haptics*, vol. 11, no. 1, pp. 30–38, Jan. 2018.

[12] R. Velazquez, E. Pissaloux, M. Hafez, and J. Szewczyk, "A low-cost highly-portable tactile display based on shape memory alloy micro-actuators," in *IEEE Symposium on Virtual Environments, Human-Computer Interfaces and Measurement Systems, 2005.*, Jul. 2005, pp. 6 pp.–.

[13] F. Vidal-Verdu and M. Hafez, "Graphical Tactile Displays for Visually-Impaired People," *IEEE Transactions on Neural Systems and Rehabilitation Engineering*, vol. 15, no. 1, pp. 119–130, Mar. 2007.

[14] "Bristol Braille Technology – Braille is literacy, education and employment," https://bristolbraille.org/.

[15] C. Loconsole, D. Leonardis, M. Gabardi, and A. Frisoli, "BrailleCursor: An Innovative Refreshable Braille Display Based on a Single Sliding Actuator and Simple Passive Pins," in *2019 IEEE World Haptics Conference (WHC)*, Jul. 2019, pp. 139–144.

[16] M. Fink and C. Prada, "Acoustic time-reversal mirrors," *Inverse Problems*, vol. 17, no. 1, p. R1, Feb. 2001.

[17] C. Hudin, J. Lozada, and V. Hayward, "Localized Tactile Feedback on a Transparent Surface through Time-Reversal Wave Focusing," *IEEE Transactions on Haptics*, vol. 8, no. 2, pp. 188–198, Apr. 2015.

[18] G. Reardon, D. Goetz, M. Linnander, and Y. Visell, "Rendering Dynamic Source Motion in Surface Haptics via Wave Focusing," *IEEE Transactions on Haptics*, vol. 16, no. 4, pp. 602–608, Oct. 2023.

[19] M. R. Bai and Y. K. Tsai, "Impact localization combined with haptic feedback for touch panel applications based on the time-reversal approach," *The Journal of the Acoustical Society of America*, vol. 129, no. 3, pp. 1297–1305, Mar. 2011.

[20] D. P. Holmes and A. J. Crosby, "Snapping Surfaces," *Advanced Materials*, vol. 19, no. 21, pp. 3589–3593, Nov. 2007.

[21] S. Shan, S. H. Kang, J. R. Raney, P. Wang, L. Fang, F. Candido, J. A. Lewis, and K. Bertoldi, "Multistable Architected Materials for Trapping Elastic Strain Energy," *Advanced Materials*, vol. 27, no. 29, pp. 4296–4301, Aug. 2015.

[22] J. Y. Chung, A. Vaziri, and L. Mahadevan, "Reprogrammable Braille on an elastic shell," *Proceedings of the National Academy of Sciences*, vol. 115, no. 29, pp. 7509–7514, Jul. 2018.

[23] W. AG, "Disc magnet 1,5 x 0,5 mm, Nickel-plated," https://www.supermagnete.de/eng/disc-magnets-neodymium/disc-magnet-1.5mm-0.5mm_S-1.5-0.5-N.

[24] L. E. Kinsler, A. R. Frey, A. B. Coppens, and J. V. Sanders, "Chapter 6.2," in *Fundamental of Acoustics*, 4th ed. John Wiler & Sons, Jan. 2000, p. 560.

[25] M. Lott and P. Roux, "Effective impedance of a locally resonant metasurface," *Physical Review Materials*, vol. 3, no. 6, p. 065202, Jun. 2019.

[26] K. F. Graff, "Chapter 4.2," in *Wave Motion in Elastic Solids*. New York: Courrier Dover Publications, 1991, p. 576.

[27] P. A. Deymier, Ed., *Acoustic Metamaterials and Phononic Crystals*, ser. Springer Series in Solid-State Sciences. Berlin, Heidelberg: Springer Berlin Heidelberg, 2013, vol. 173.

[28] T. Daunizeau, D. Gueorguiev, S. Haliyo, and V. Hayward, "Phononic Crystals Applied to Localised Surface Haptics," *IEEE Transactions on Haptics (ToH)*, vol. 14, no. 3, pp. 668–674, 2021.

[29] Y. Xiao, J. Wen, and X. Wen, "Flexural wave band gaps in locally resonant thin plates with periodically attached spring–mass resonators," *Journal of Physics D: Applied Physics*, vol. 45, no. 19, p. 195401, May 2012.

[30] P. Karban, D. Pánek, and J. Kaska, "Open-source platform for simulation of physical fields: Agros," *Journal of Computational and Applied Mathematics*, vol. 465, p. 116589, Sep. 2025.

[31] C. Hudin, "Local friction modulation using non-radiating ultrasonic vibrations," in *2017 IEEE World Haptics Conference (WHC)*, Jun. 2017, pp. 19–24.